Editors' Suggestion

Periodic Wave Trains in Nonlinear Media: Talbot Revivals, Akhmediev Breathers, and Asymmetry Breaking

Georgi Gary Rozenman,[1,2] Wolfgang P. Schleich,[3,4] Lev Shemer,[5] and Ady Arie[2]
[1]Raymond and Beverly Sackler School of Physics and Astronomy, Faculty of Exact Sciences, Tel Aviv University, Tel Aviv 69978, Israel
[2]School of Electrical Engineering, Iby and Aladar Fleischman Faculty of Engineering, Tel Aviv University, Tel Aviv 69978, Israel
[3]Institut für Quantenphysik and Center for Integrated Quantum Science and Technology (IQ^{ST}), Universität Ulm, 89081 Ulm, Germany
[4]Hagler Institute for Advanced Study at Texas A&M University, Texas A&M AgriLife Research, Institute for Quantum Science and Engineering (IQSE), and Department of Physics and Astronomy, Texas A&M University, College Station, Texas 77843-4242, USA
[5]School of Mechanical Engineering, Faculty of Engineering, Tel Aviv University, Tel Aviv 69978, Israel

(Received 1 March 2022; accepted 7 April 2022; published 27 May 2022)

We study theoretically and observe experimentally the evolution of periodic wave trains by utilizing surface gravity water wave packets. Our experimental system enables us to observe both the amplitude *and* the phase of these wave packets. For low steepness waves, the propagation dynamics is in the linear regime, and these waves unfold a Talbot carpet. By increasing the steepness of the waves and the corresponding nonlinear response, the waves follow the Akhmediev breather solution, where the higher frequency periodic patterns at the fractional Talbot distance disappear. Further increase in the wave steepness leads to deviations from the Akhmediev breather solution and to asymmetric breaking of the wave function. Unlike the periodic revival that occurs in the linear regime, here the wave crests exhibit self acceleration, followed by self deceleration at half the Talbot distance, thus completing a smooth transition of the periodic pulse train by half a period. Such phenomena can be theoretically modeled by using the Dysthe equation.

DOI: 10.1103/PhysRevLett.128.214101

Introduction.—The optical Talbot effect, discovered by Henry Fox Talbot in the 19th century [1], is the revival of a periodic light pattern at periodic distances (Talbot distances denoted $x_T = 2T^2/\lambda$, where T and λ are the period of the diffraction grating and optical wavelength) from the input plane [2]. Moreover, higher frequency periodic patterns appear at fractional Talbot distances. The fractional Talbot distance is given by p_{x_T}/q, where p and q are prime numbers and the oscillation frequency is q times faster [3].

Because of the quantum mechanical wave nature of particles, such diffraction effects have also been observed with matter waves [4–6], which are similar to those in the case of light waves [7].

Ever since, this phenomenon in quantum physics, which is closely related to the Talbot effect, has been extensively studied in many quantum mechanical systems [8–18]. For instance, a quantum carpet can be constructed from an evolution of the wave function of a single particle in an infinite square well [19–21].

The evolution of periodic wave trains was also extended to the nonlinear regime. Specifically, Akhmediev [22–24] derived an analytic solution, known as Akhmediev breather, to the nonlinear Schrödinger equation (NLSE) with third order nonlinear response, which was recently studied experimentally in a cubic nonlinear optical medium [25,26]. One of the interesting predictions [27], which was not observed experimentally until now, is that when the nonlinear effects become significant, the faster oscillations at the fractional Talbot distances disappear.

In this Letter, we study the evolution of periodic wave trains for different levels of nonlinearity, by using surface gravity water wave pulses. The linear wave equation for these waves is analogous to the Schrödinger equation for quantum wave packets, and to the paraxial Helmholtz equation for optical beams [28–34]. The nonlinear terms of the Schrödinger equations can be controlled by setting the steepness of the initial wave packet. At low steepness, the propagation dynamics along the test section is approximately linear, thus we observe the familiar Talbot carpet, including the higher frequency oscillations at fractional Talbot distances. For higher steepness, we observe the disappearance of these fractional orders, in correspondence with Akhmediev's solution. But when we further increase the steepness, asymmetric breaking of the wave packet is observed, i.e., the wave crests accelerate and then decelerate at half the Talbot distance leading to a shift of the pulse

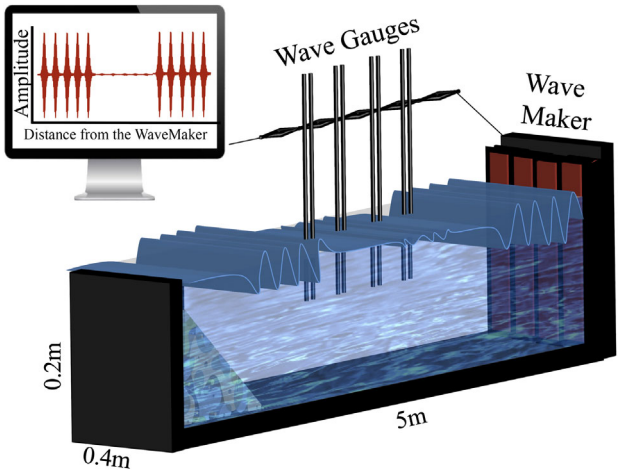

FIG. 1. Experimental setup for observing the linear and nonlinear Talbot effect with surface gravity water waves.

train by half a period. This behavior is significantly different with respect to the familiar disappearance and revival of the wave crests in the linear case. This phenomenon can no longer be described using the analytic Akhmediev breather, but is in agreement with numerical predictions based on the Dysthe equation [32,35].

Scheme.—The observation of the linear and nonlinear Talbot effect is performed in a 5 m long, 0.4 m wide, and 0.2 m deep water-wave tank with a computer controlled wave maker, see Fig. 1. A wave energy absorbing beach is placed at the other end of the water tank. To eliminate the effect of the beach, precise measurements of the water surface elevation are carried out by wave gauges at distances not exceeded 4.5 m from the wave maker.

For surface gravity water waves with high steepness, we apply the spatial version of the Dysthe equations [32,35,36]

$$\frac{\partial A}{\partial \xi}+i\frac{\partial^2 A}{\partial \tau^2}+i|A|^2A+8\varepsilon|A|^2\frac{\partial A}{\partial \tau}+2\varepsilon A^2\frac{\partial A^*}{\partial \tau}+4i\varepsilon A\frac{\partial \Phi}{\partial \tau}\bigg|_{Z=0}=0, \tag{1}$$

$$4\frac{\partial^2\Phi}{\partial \tau^2}+\frac{\partial^2\Phi}{\partial Z^2}=0 \qquad (Z<0),$$
$$\frac{\partial \Phi}{\partial Z}\bigg|_{Z=0}=\frac{\partial |A|^2}{\partial \tau}, \qquad \frac{\partial \Phi}{\partial Z}\bigg|_{Z\to-\infty}=0 \tag{2}$$

for the normalized amplitude envelope $A(\tau,\xi)$ and the envelope of the self-induced velocity potential $\Phi(\tau,Z)$ in the moving frame.

Here the scaled dimensionless variables ξ, τ, and Z are related to the propagation coordinate x, the time t, and the vertical coordinate z by $\xi\equiv\varepsilon^2k_0x$, $\tau\equiv\varepsilon\omega_0(x/c_g-t)$, and $Z\equiv\varepsilon k_0z$. The carrier wave number k_0 and the angular carrier frequency ω_0 satisfy the deep-water dispersion relation $\omega_0^2=k_0g$, with g being the gravitational acceleration, and define the group velocity $c_g\equiv\omega_0/2k_0$. Moreover, $\Phi\equiv\phi/(\omega_0a_0^2)$ denotes the dimensionless velocity potential.

We recall that for moderate nonlinearites, Eq. (1) reduces to a nonlinear Schrödinger equation [30]

$$i\frac{\partial A}{\partial \xi}=\frac{\partial^2 A}{\partial \tau^2}+|A|^2A \tag{3}$$

for which a general Akhmediev solution of the cubic NLSE, expressed in terms of the Jacobi elliptic functions cn, sn, and dn is given [37] by

$$A(\tau,\xi)=\kappa\frac{\alpha(\tau)\mathrm{dn}(\kappa\xi,1/\kappa)+\frac{i}{k}\mathrm{sn}(\kappa\xi,1/\kappa)}{1-\alpha(\tau)\mathrm{cn}(\kappa\xi,1/\kappa)}\exp(i\xi), \tag{4}$$

where $\alpha(\tau)=\sqrt{[1/(1+\kappa)]}\mathrm{cn}(\sqrt{2\kappa}\tau,\sqrt{[(\kappa-1)/2\kappa]})$ and $\kappa>1$ is a modification parameter [37].

The complex amplitude envelope $A\equiv|A|\exp(i\varphi)$ determines the variation in time and space of the surface elevation

$$\eta(t,x)\equiv a_0A(t,x)\cos[k_0x-\omega_0t], \tag{5}$$

including the carrier wave, where a_0 is the maximum amplitude of the envelope.

For observing both the linear and nonlinear Talbot effect, the wave maker at $x=0$ is prescribed to generate the temporal multilobe periodic surface elevation in the form of the Akhmediev wave

$$A(\tau,0)=\kappa\frac{\alpha(\tau)}{1-\alpha(\tau)} \tag{6}$$

with the period $\Delta\tau=(4/\sqrt{\kappa})K(\sqrt{[(\kappa-1)/2k]})$, where $K(m)$ is the complete elliptic integral of the first kind [38].

Linear Talbot effect.—First, we study the propagation dynamics of water waves induced by this initial profile $A(\tau,0)$, Eq. (6), in a linear regime, when the wave steepness $\varepsilon=k_0a_0$ is low, $\varepsilon<0.1$. In this case the envelope $A(\tau,\xi)$ obeys the equation [30,39]

$$i\frac{\partial A}{\partial \xi}=\frac{\partial^2 A}{\partial \tau^2} \tag{7}$$

that is similar to the one-dimensional time-dependent Schrödinger equation of a free particle. However, the roles of time and space are interchanged.

We measure the elevation $\eta(t,x)$ at 40 spatial locations and 7200 temporal points (with an averaging of 10). In Fig. 2 we present the amplitude $|A(t,x)|$ observed (a) in our setup together with the simulations (d) and (g) based on Eq. (7) for $\varepsilon=0.026$. We observe that the revival of the periodic pattern occurs at $x_T=(4.08\pm0.10)$ m, which

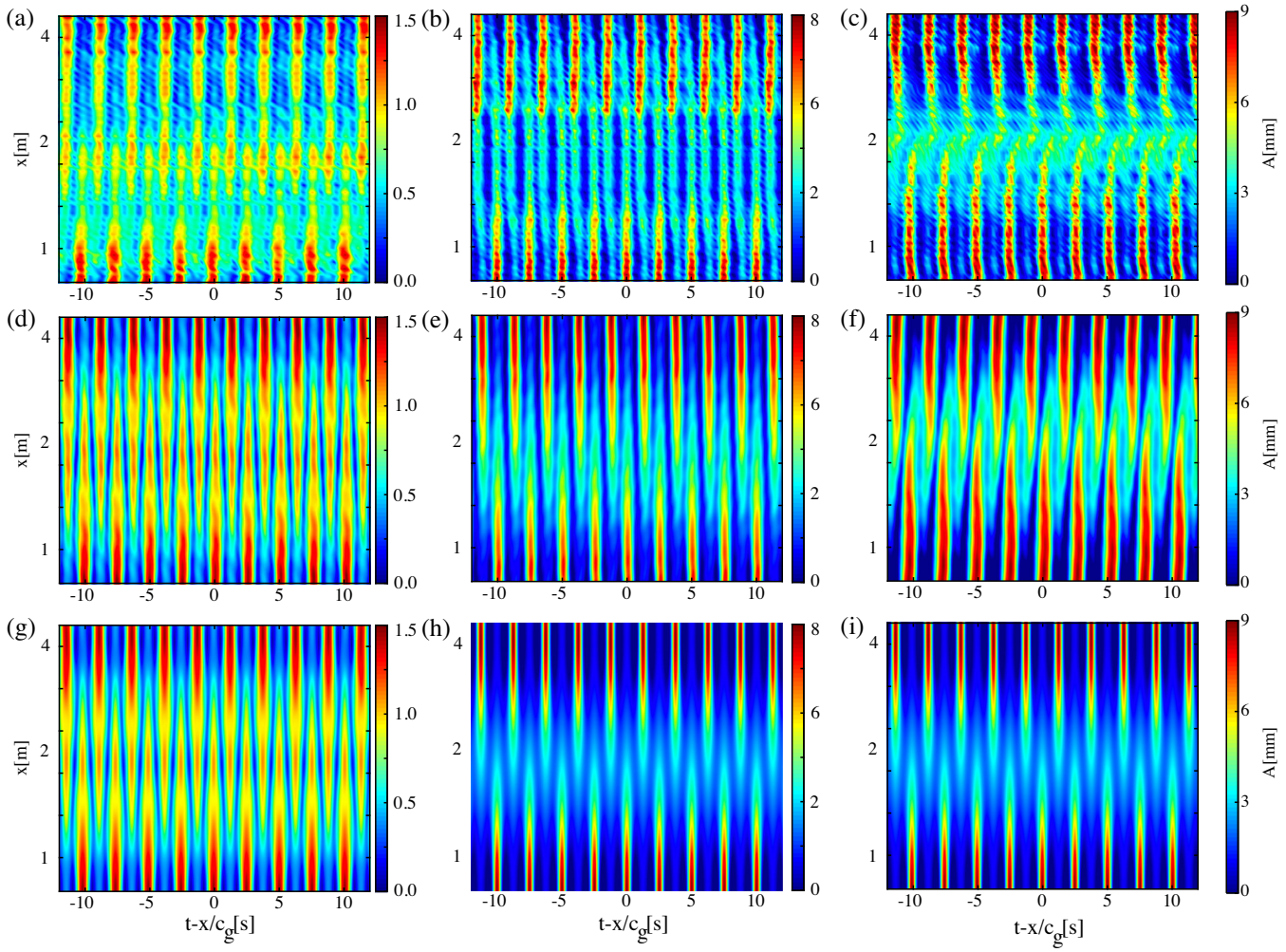

FIG. 2. Space-time profile of the envelope amplitude $A(t,x)$ induced by the Akhmediev wave, Eq. (6), with $\kappa = 2$ for linear, nonlinear, and highly nonlinear waves. (a) $a_0 = 1.5$ mm and $\omega_0 = 13$ [rad/s] ($\varepsilon = 0.026$). (b) $a_0 = 8$ mm and $\omega_0 = 15$ [rad/s] ($\varepsilon = 0.18$). (c) $a_0 = 9$ mm and $\omega_0 = 17$ [rad/s] ($\varepsilon = 0.265$). The theoretical plots in (d)–(f) are simulations based on Eq. (1) for the corresponding parameters in (a)–(c), i.e., steepness of $\varepsilon = 0.026$, 0.18, 0.265. (g) Simulation based on the linear Schrödinger equation, Eq. (7) for $\varepsilon = 0.026$, (h) analytical plot for $\varepsilon = 0.18$ based on Eq. (4), (i) numerical plot for $\varepsilon = 0.265$ based on Eq. (3).

agrees with the corresponding simulations $x_{T_s} = 4.12$ m and analytical calculation $x_{T_a} = 4.05$ m [40]. In addition, the fractional Talbot effect having the period $\frac{1}{2}x_T$ is also observed around $x = (1.90 \pm 0.10)$ m.

Next, using the Hilbert transform [41,42], we extract the phase $k_0 x - \omega_0 t + \varphi(t,x)$ of the surface elevation $\eta = \eta(t,x)$. After removing the carrier phase $k_0 x - \omega_0 t$, the complete space-time profile of $\varphi(t,x)$ is presented in Fig. 3(a) together with the corresponding simulations, shown in Figs. 3(d) and 3(g). Thus, we have successfully observed the linear Talbot effect for both the amplitude *and* the phase.

Nonlinear Talbot effect.—We further study the Talbot effect in the nonlinear regime. For this purpose, the wave maker at $x = 0$ is again prescribed to generate the temporal multilobe periodic surface elevation given by Eq. (6) but now with a relatively large steepness $\varepsilon = 0.18$ where nonlinear effects come into play. The intensity distribution of the solution with $\kappa = 2$ is displayed in Fig. 2(b) alongside the theoretical results, predicted by Eq. (1), shown in Fig. 2(e). We observe that the solution exhibits the self-imaging Talbot carpet which appears at Talbot distances, and it is π-phase shifted. The wave dynamics for $\varepsilon = 0.18$ is governed by the nonlinear response. The solution corresponds to the eigenmode of NLSE, given by Eq. (4) and it propagates in a nonlinear medium. We experimentally observe that for such nonlinear waves, the fractional revivals, which are clearly seen in Figs. 2(a), 2(d), and 2(g) are absent, as was recently predicted in a theoretical study [27]. However, one can see that even at intermediate nonlinearities, the analytical solution based on Eq. (3), which is shown in Fig. 2(h) does not describe accurately the experimental result shown in 2(b), whereas the simulation based on Eq. (1) in Fig. 2(e) yields a more

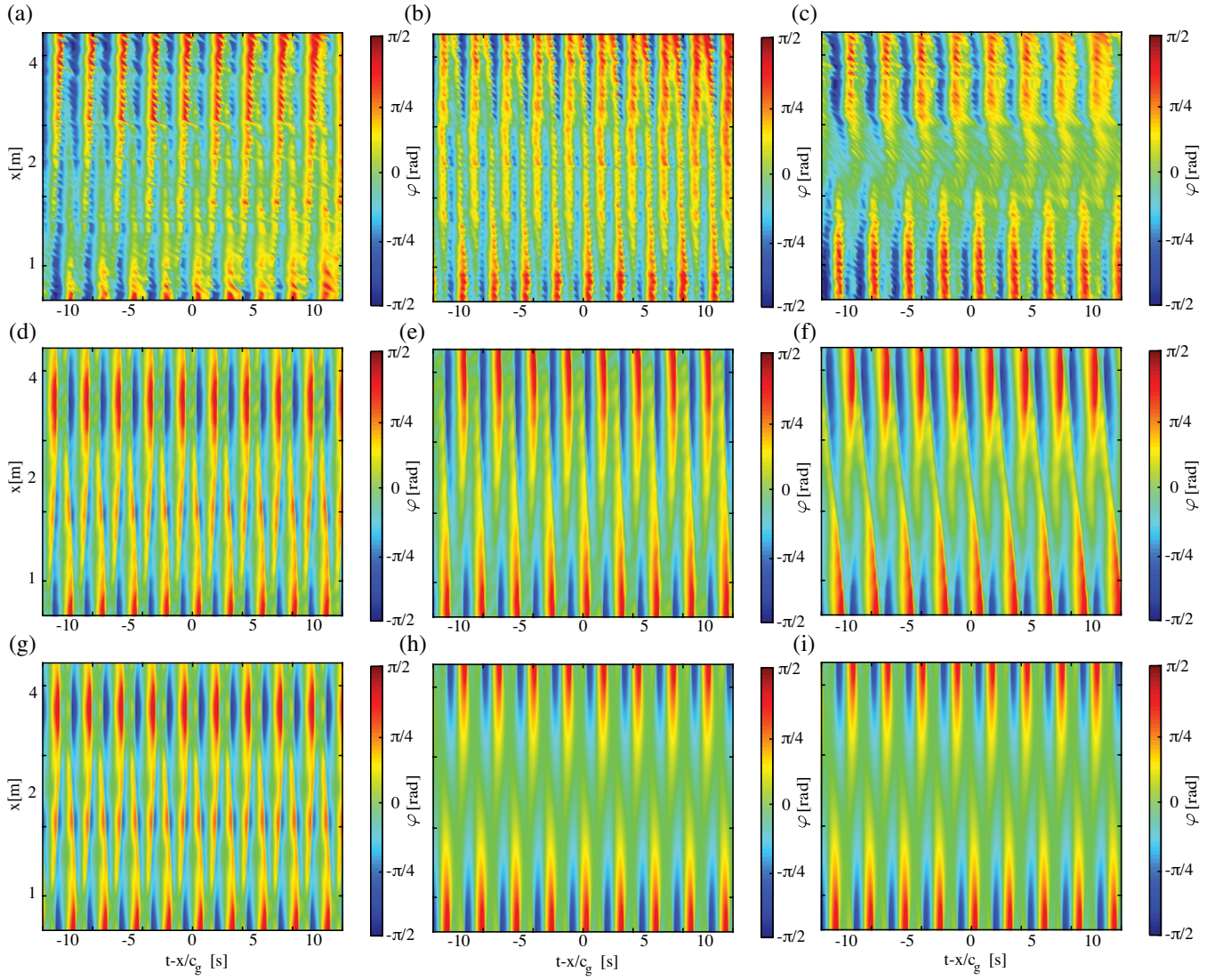

FIG. 3. Space-time profile of the envelope phase $\varphi(t,x)$ induced by the Akhmediev wave, Eq. (6), with $\kappa = 2$ for linear, nonlinear, and highly nonlinear waves. (a) $a_0 = 1.5$ mm and $\omega_0 = 13$ [rad/s] ($\varepsilon = 0.026$). (b) $a_0 = 8$ mm and $\omega_0 = 15$ [rad/s] ($\varepsilon = 0.18$). (c) $a_0 = 9$ mm and $\omega_0 = 17$ [rad/s] ($\varepsilon = 0.265$). The theoretical plots in (d)–(f) are simulations based on Eq. (1) for the corresponding parameters in (a)–(c), i.e., steepness of $\varepsilon = 0.026$, 0.18, 0.265. (g) Simulation based on the linear Schrödinger equation, Eq. (7) for $\varepsilon = 0.026$, (h) analytical plot for $\varepsilon = 0.18$ based on Eq. (4), (i) numerical plot for $\varepsilon = 0.265$ based on Eq. (3).

accurate prediction. For instance, it indicates the uneven gap in the formed dark canals at $x = 2$ m. The mentioned differences are further strengthened by observing the longitudinal differences in the phase pattern with the experimental result shown in Fig. 3(a). The simulation based on Eq. (1) and shown in Fig. 3(b) predicts these characteristics while the analytical result shown in Fig. 3(h) has shorter longitudinal lobes.

Finally, we increase the wave steepness to $\varepsilon = 0.265$ and study the evolution of periodic wave trains in this highly nonlinear regime. As seen in Fig. 2(c), we observe extraordinary behaviour of wave packets which has not been reported before either theoretically or experimentally [27]. Namely, at half the Talbot distance, around $x = 2$–3 m the envelope wave amplitude $A(t,x)$ breaks asymmetrically and new canals are formed. In that particular region, each lobe slightly self-accelerates and each new emerging lobe slightly decelerates back to the same group velocity as the lobes found at the origin. The fractional disappearance and revivals, observed in Fig. 2(a) for low steepness, are absent, as depicted in Fig. 2(b). Instead, we observe a continuous shift of the wave crests by half of the period. These results are successfully verified by solving Eqs. (1) and (2) numerically, as shown in Fig. 2(f), and compared to the numerical solution of the third-order nonlinear Schrödinger equation, that is Eq. (3) [27], shown in Fig. 2(i). Thus, Eqs. (1) and (2), which include high-order terms proportional to ε, describe accurately the dynamics of the

envelope amplitude $A(t,x)$ in the nonlinear regime, in particular the Talbot effect. These asymmetric properties are also observed in the phase in Fig. 3(c) and are modeled numerically in 3(f) by solving Eqs. (1) and (2).

In conclusion, we have studied and observed the linear and nonlinear Talbot effect for both the amplitude and the phase of surface gravity water waves originating from the Akhmediev wave. In addition, beyond the linear regime we have observed the disappearance of the fractional revivals. Finally, for even higher steepness of water waves, the fractional Talbot effect (at $x = 1.9$ m) is absent and a self-accelerating pattern of the wave crest is observed, in contrast to the familiar disappearance and revival pattern in the linear case. We also emphasize that our experimental setup is not limited to freely propagating waves and it is possible to study this phenomena in the presence of a linear potential [30,31].

We anticipate that the evolution of periodic patterns that we observed here should occur for other types of waves, e.g., optical waves, where at low intensity they will exhibit revivals at integer and fractional Talbot distances, followed by the disappearance of the higher periodic structures at fractional distances for a Kerr nonlinear medium, and finally deviations from the Akhemediev breather solution when higher order nonlinear terms come into play.

We thank Maxim A. Efremov, Matthias Zimmermann, and Anatoliy Khait for fruitful discussions help and support, and Tamir Ilan for technical support and advice. We also thank the CLEO-2021 conference where we first presented the results that led to this Letter [43]. This work is supported by DIP, the German-Israeli Project Cooperation (AR 924/1-1, DU 1086/2-1) supported by the DFG, the Israel Science Foundation (Grants No. 1415/17, No. 508/19). W. P. S. is grateful to Texas A&M University for a Faculty Fellowship at the Hagler Institute for Advanced Study at the Texas A&M University as well as to the Texas A&M AgriLife Research. The research of the IQST is financially supported by the Ministry of Science, Research and Arts Baden-Württemberg.

[1] H. F. Talbot, Philos. Mag. **9**, 401 (1836).
[2] L. Rayleigh, Philos. Mag. **11**, 196 (1881).
[3] M. Berry and S. Klein, J. Mod. Opt. **43**, 2139 (1996).
[4] J. Wen, Y. Zhang, and M. Xiao, Adv. Opt. Photonics **5**, 83 (2013).
[5] L. Deng, E. W. Hagley, J. Denschlag, J. E. Simsarian, M. Edwards, Ch. W. Clark, K. Helmerson, S. L. Rolston, and W. D. Phillips, Phys. Rev. Lett. **83**, 5407 (1999).
[6] J. Ruostekoski, B. Kneer, W. P. Schleich, and G. Rempe, Phys. Rev. A **63**, 043613 (2001).
[7] S. Nowak, Ch. Kurtsiefer, T. Pfau, and C. David, Opt. Lett. **22**, 1430 (1997).
[8] A. E. Kaplan, I. Marzoli, W. E. Lamb, Jr., and W. P. Schleich, Phys. Rev. A **61**, 032101 (2000).
[9] M. R. Barros, A. Ketterer, O. J. Farias, and S. P. Walborn, Phys. Rev. A **95**, 042311 (2017).
[10] X. B. Song, H. B. Wang, J. Xiong, K. Wang, X. Zhang, K. H. Luo, and L. A. Wu, Phys. Rev. Lett. **107**, 033902 (2011).
[11] O. J. Farias, F. deMelo, P. Milman, and S. P. Walborn, Phys. Rev. A **91**, 062328 (2015).
[12] J. Banerji, Contemp. Phys. **48**, 157 (2007).
[13] A. Stibor, A. Stefanov, F. Goldfarb, E. Reiger, and M. Arndt, New J. Phys. **7**, 224 (2005).
[14] K. I. Oskolkov, Banach Cent. Pub. **72**, 189 (2006).
[15] W. Loinaz and T. J. Newman, J. Phys. A **32**, 8889 (1999).
[16] D. M. Meekhof, C. Monroe, B. E. King, W. M. Itano, and D. J. Wineland, Phys. Rev. Lett. **76**, 1796 (1996).
[17] J. Parker and C. R. Stroud, Phys. Rev. Lett. **56**, 716 (1986).
[18] K. Leo, J. Shah, E. O. Göbel, T. C. Damen, S. Schmitt-Rink, W. Schäfer, and K. Köhler, Phys. Rev. Lett. **66**, 201 (1991).
[19] M. V. Berry, I. Marzoli, and W. P. Schleich, Phys. World **14**, 39 (2001).
[20] F. Saif and M. Fortunato, Phys. Rev. A **65**, 013401 (2001).
[21] P. Kazemi, S. Chaturvedi, I. Marzoli, R. F. O'Connell, and W. P. Schleich, New J. Phys. **15**, 013052 (2013).
[22] N. Akhmediev, V. Eleonskii, and N. Kulagin, Theor. Math. Phys. **72**, 809 (1987).
[23] A. Chabchoub, B. Kibler, C. Finot G. Millot, M. Onorato, J. Dudley, and A. V. Babanin, Ann. Phys. (Amsterdam) **361**, 490 (2015).
[24] J. Dudley, F. Dias, F. Erkintalo, M. Erkintalo, and G. Genty, Nat. Photonics, **8**, 755 (2014).
[25] R. Schiek, Opt. Express **29**, 15830 (2021).
[26] In Ref. [25] the emphasis was on the optical cubic nonlinearity, hence asymmetry breaking that is observed in the present Letter and which originates from other nonlinear terms in the Dysthe equations was not studied. Furthermore, Ref. [25] reports on measurements of the output plane as a function of the beam intensity, whereas we have followed the wave dynamics in both time and space, for several values of steepness and have measured the global phase.
[27] Y. Zhang, M. R. Belic, H. Zheng, H. Chen, C. Li, J. Song, and Y. Zhang, Phys. Rev. E **89**, 032902 (2014).
[28] S. Fu, Y. Tsur, J. Zhou, L. Shemer, and A. Arie, Phys. Rev. Lett. **115**, 034501 (2015).
[29] S. Fu, Y. Tsur, J. Zhou, L. Shemer, and A. Arie, Phys. Rev. Lett. **115**, 254501 (2015).
[30] G. G. Rozenman, S. Fu, A. Arie, and L. Shemer, MDPI-Fluids **4**, 96 (2019), https://www.mdpi.com/2311-5521/4/2/96.
[31] G. G. Rozenman, M. Zimmermann, M. A. Efremov, W. P. Schleich, L. Shemer, and A. Arie, Phys. Rev. Lett. **122**, 124302 (2019).
[32] L. Shemer and B. Dorfman, Nonlinear Processes Geophys. **15**, 931 (2008).
[33] D. Weisman, C. M. Carmesin, G. G. Rozenman, M. A. Efremov, L. Shemer, W. P. Schleich, and A. Arie, Phys. Rev. Lett. **127**, 014303 (2021).
[34] M. R. Gonçalves, G. G. Rozenman, M. Zimmermann, M. A. Efremov, W. B. Case, A. Arie, L. Shemer, and W. P. Schleich, Appl. Phys. B **128**, 51 (2022).
[35] K. B. Dysthe, Proc. R. Soc. A **369**, 105 (1979).

[36] G. G. Rozenman, L. Shemer, and A. Arie, Phys. Rev. E **101**, 050201 (2020).
[37] N. Akhmediev, V. Eleonskii, and N. Kulagin, Theor. Math. Phys. **72**, 809 (1987).
[38] M. Abramowitz and I. A. Stegun, *Handbook of Mathematical Functions* (Dover, New York, 1970).
[39] C. C. Mei, *The Applied Dynamics of Ocean Surface Waves* (Wiley-Interscience, Singapore, 1983).
[40] The exact expression derived by Lord Rayleigh for the primary image of the optical Talbot distance is $z_T = \lambda/(1-\sqrt{1-\lambda^2/a^2})$. In surface gravity waves this distance is given in temporal units by $t_T = T/(1-\sqrt{1-T^2/\Delta t^2})$, where T is the period of the carrier wave and Δt is the period between envelope lobes. Hence, the Talbot distance for the secondary image mentioned in this Letter is given by $x_T = \frac{1}{2} c_g t_T$, where c_g is the group velocity.
[41] F. W. King, *Hilbert Transforms* (Cambridge University Press, Cambridge, England, 2009), Vol. 1.
[42] MATLAB Hilbert Transform package (https://www.mathworks.com/help/signal/ug/hilbert-transform.html).
[43] G. G. Rozenman, L. Shemer, M. Zimmermann, M. Efremov, W. Schleich, and A. Arie, *Proceedings of the Conference on Lasers and Electro-Optics* (Optica Publishing Group, 2021), paper FM3I.5.